

Structure of nanocomposites grown by electron beam induced deposition

Milos Toth¹, Juntao Li², Vasiliki Tileli², Kathleen A. Dunn², Charlene J. Lobo¹ and Bradley L. Thiel²

¹*FEI Company, 5350 NE Dawson Creek Dr., Hillsboro, OR 97124, USA.*

²*College of Nanoscale Science and Engineering, University at Albany-SUNY, 251 Fuller Road, Albany, NY, 12203, USA.*

Gas-mediated electron beam induced deposition (EBID) [1-3] is a direct-write technique with sub-10 nm spatial resolution. Most materials grown by EBID are nanocomposites comprised of high purity crystallites with typical diameters in the range of 1 to 10 nm embedded in an amorphous matrix. The matrix is usually highly impure and the deposit nanostructure often limits the functionality of materials grown by EBID. We show that the degree of deposit crystallinity and the crystallite size distribution evolve during growth, and that these changes scale with electron energy density delivered to the deposits during EBID. Furthermore, in some systems, the crystallites intermix with the substrate. The intermixing process is shown to be athermal, electron-activated and rate limited by mass transport inside the solid. The changes in nanostructure reported here scale with growth parameters and can be induced by post-growth electron irradiation of the deposits, enabling control over the nanostructure and functionality of materials grown by EBID.

The effects reported here were observed in a range of nanocomposites comprised of metallic and dielectric nanocrystallites such as Pt and WO₃. Room temperature EBID was performed using two methods: local injection of precursors such as (CH₃)₃CH₃C₅H₄Pt into a high vacuum scanning electron microscope by a capillary-style gas injection system [1], and by using gases such as WF₆ as the background gas in environmental scanning electron microscopy [2-3]. The substrates were p-type Si (100), plasma-cleaned prior to growth, yielding an approximately 5 nm thick SiO_x layer. The electron fluence and flux, and post-growth processing were controlled by varying the beam current, growth time, and the diameter of a stationary 20 keV electron beam with a top-hat electron flux profile.

Examples of the abovementioned changes in nanostructure are shown in the figures. Fig. 1 and 2 show secondary electron images, TEM images and selected area diffraction (SAD) patterns from deposits fabricated using WF₆ as a function of growth time. The crystallites are body-centered cubic WO₃ with a lattice constant of $a=7.521\text{\AA}$. The TEM data show an increase in deposit crystallinity and grain size with growth time. Fig. 3 and 4 show images & SAD patterns of deposits grown from (CH₃)₃CH₃C₅H₄Pt as a function of electron beam diameter; comprised of crystallites of face-centered cubic Pt with a lattice constant of $a=3.92\text{\AA}$. The degree of deposit crystallinity scales inversely with the diameter of the electron beam used for EBID. Fig. 5 (a-d) shows TEM images of the interface between each of the four deposits A1-A4 and the SiO_x/Si substrate, and an analogous image (e) taken from a region adjacent to deposits. The thickness of the SiO_x layer under the deposits decreases systematically from ~2.5 nm to 1.6 nm. These and analogous data from deposits that were post-processed by an electron beam in high vacuum will be used to discuss possible mechanisms behind the observed changes in nanostructure and implications for the growth of functional materials by EBID.

[1] I. Utke, P. Hoffmann, and J. Melngailis, *J. Vac. Sci. B* **26**, 1197-1276 (2008).

[2] M. Toth, C.J. Lobo, W.R. Knowles, M.R. Phillips, M.T. Postek, A.E. Vladar, *Nano Lett.* **7**, 525-530 (2007).

[3] J. Li, M. Toth, V. Tileli, K.A. Dunn, C.J. Lobo, B.L. Thiel, *Appl. Phys. Lett.* **93**, 023130 (2008).

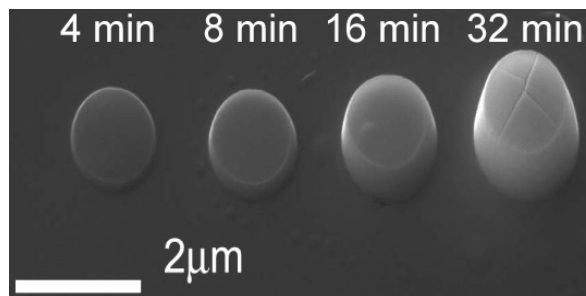


Fig. 1. SEM image (sample tilt = 52°) of deposits fabricated using WF_6 precursor and growth times of 4, 8, 16 and 32 min.

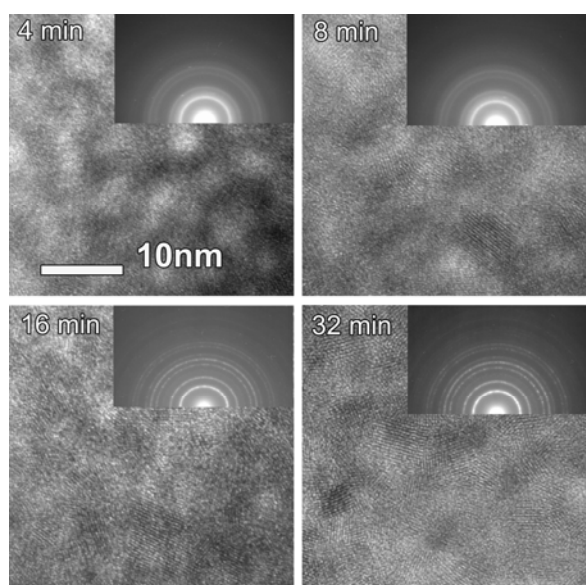


Fig. 2. Cross-sectional TEM images of the deposits shown in Fig. 1. **Insets:** selected area diffraction patterns taken from the center of each deposit.

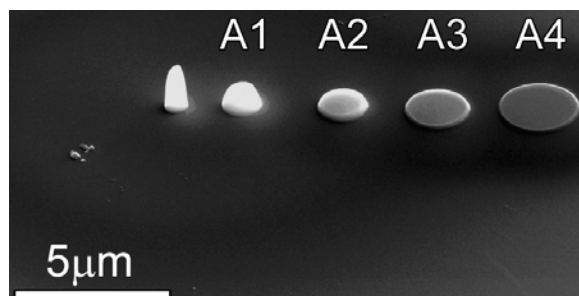


Fig. 3. SEM image (sample tilt = 52°) of deposits grown using $(\text{CH}_3)_3\text{CH}_3\text{C}_5\text{H}_4\text{Pt}$ precursor. The deposit top diameters (from left to right, “A1” to “A4”) are 850, 1410, 2020 and 2580 nm.

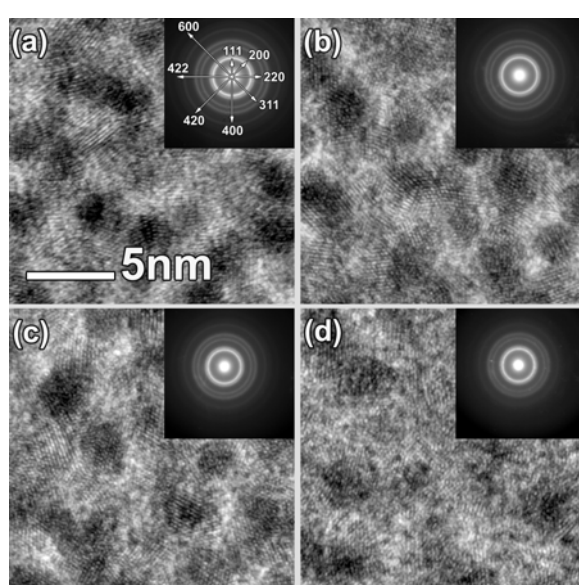


Fig. 4. (a-d) Cross-sectional TEM images of deposits A1 to A4, respectively. **Insets:** selected area diffraction patterns taken from the center of each deposit.

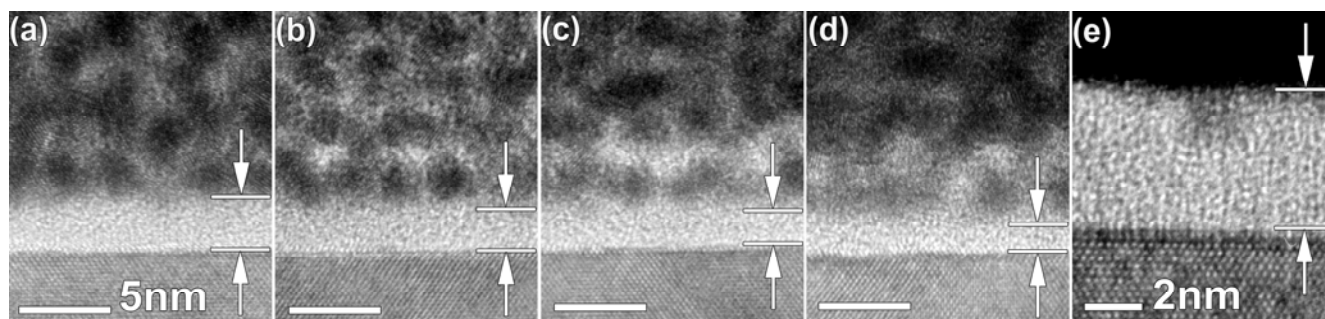


Fig. 5. Cross-sectional TEM images of the interface between the SiO_x/Si substrate and deposits A1 to A4. The SiO_x thickness in images (a) to (d) is 2.5 ± 0.1 nm, 2.2 ± 0.1 nm, 1.9 ± 0.1 nm, and 1.6 ± 0.1 nm, respectively. (e) TEM image of a SiO_x/Si substrate showing the amorphous oxide overlayer (thickness ≈ 5.4 nm) in a region adjacent to the deposits.